Minimization of self-potential survey mis-ties acquired with multiple reference locations

GEOPHYSICS, VOL. 73, NO. 2 (MARCH-APRIL 2008); P. F71–F81, 9 FIGS., 1 TABLE.
10.1190/1.2829390

Minimization of self-potential survey mis-ties acquired with multiple reference locations

Burke J. Minsley[1], Darrell A. Coles[1], Yervant Vichabian[2], and Frank Dale Morgan[1]

ABSTRACT

Self-potential (SP) surveys often involve many interconnected lines of data along available roads or trails, with the ultimate goal of producing a unique map of electric potentials at each station relative to a single reference point. Multiple survey lines can be tied together by collecting data along intersecting transects and enforcing Kirchhoff's voltage law, which requires that the total potential drop around any closed loop equals zero. In practice, however, there is often a nonzero loop-closure error caused by noisy data; traditional SP processing methods redistribute this error evenly over the measurements that form each loop. The task of distributing errors and tying lines together becomes nontrivial when many lines of data form multiple interconnected loops because the loop-closure errors are not independent, and a unique potential field cannot be determined by processing lines sequentially. We present a survey-consistent processing method that produces a unique potential field by minimizing the loop-closure errors over all lines of data simultaneously. When there are no interconnected survey loops, the method is equivalent to traditional processing schemes. The task of computing the potential field is posed as a linear inverse problem, which easily incorporates prior information about measurement errors and model constraints. We investigate the use of both l_2 and l_1 measures of data misfit, the latter requiring an iterative-solution method with increased computational cost. The l_1 method produces more reliable results when outliers are present in the data, and is similar to the l_2 result when only Gaussian noise is present. Two synthetic examples are used to illustrate this methodology, which is subsequently applied to a field data set collected as part of a geothermal exploration campaign in Nevis, West Indies.

INTRODUCTION

Geophysical surveys often consist of multiple transects of data collected on regular or irregular grids with multiple crossover points. These data are collected with the goal of uniquely defining some geophysical parameter (electrical potential, gravity, temperature, bathymetry, etc.) over the survey area. Measurements are inherently imperfect, and may be contaminated by unknown random and systematic errors. Mis-ties (also called misclosures or crossover errors) at intersection points result from the accumulation of these imperfect measurements along different survey lines. A successful analysis of the measured data will uniquely define the underlying field values such that they best represent the data, subject to available measurement-error statistics or model constraints.

Several previous studies have addressed the geophysical mis-tie problem from various perspectives. For example, Cowles (1938) uses an electrical-network analogy to solve the misclosure problem for geophysical traverses using least-squares methods similar to those discussed in this paper. Foster et al. (1970) discuss the discrepancy in aeromagnetic data at the intersection of survey lines caused by systematic errors in a statistical framework. Johnson (1971) utilizes the uncertainty in a vessel's position when accounting for discrepancies at crossing points in marine geophysical-survey lines. Prince and Forsyth (1984) present a method to minimize crossover errors in marine-gravity data using a least-squares approach that determines an optimal set of constant correction terms for each survey line. Finally, Bandy et al. (1990) discuss a direct method for determining corrections to geophysical-survey lines that least distorts the original survey in addition to minimizing mis-ties.

In this paper, we expand on several of these concepts to present an efficient method for processing self-potential (SP) data collected

Manuscript received by the Editor 4 July 2007; revised manuscript received 11 October 2007; published online 12 February 2008.
[1]Massachusetts Institute of Technology, Department of Earth, Atmospheric and Planetary Sciences, Cambridge, Massachusetts, U.S.A. E-mail: minsley@mit.edu; dcoles@erl.mit.edu; morgan@erl.mit.edu.
[2]Formerly SP International, Inc.; presently North Dighton, Massachusetts, U.S.A. E-mail: yerv@juno.com.

with complicated survey geometries. SPs refer to passively measured electric potentials that are generated through coupling with various subsurface-flow phenomena in the earth, and have been utilized in fields such as mineral exploration (Sato and Mooney, 1960; Sivenas and Beales, 1982), geothermal exploration (Corwin and Hoover, 1979; Fitterman and Corwin, 1982), environmental and geotechnical applications (Corwin, 1990; Naudet et al., 2004; Minsley et al., 2007b), and hydrogeology (Bogoslovsky and Ogilvy, 1973; Revil et al., 2002; Suski et al., 2004).

While there are various data-acquisition techniques, the goal of an SP survey is to produce a map of the electric-potential field relative to a single reference station. In what we term traditional processing methods, multiple lines of data collected with different reference stations are tied together by determining the potentials along each line and then measuring the potential difference between lines. The potential drop around survey lines that form a closed loop should equal zero, but this is often not achieved because of measurement errors. In this case, the nonzero closure error is distributed among the measurements that form the loop. These traditional methods are straightforward when the survey geometry is simple, but are inadequate for more complicated geometries that involve multiple intersection points and interconnected loops.

Although this methodology focuses on application to SP signals, the techniques can be easily adapted to various geophysical-survey types, particularly potential-field problems. There is also a similarity between the methods discussed here and previously developed techniques for determining relative seismic traveltimes using multichannel, crosscorrelation methods (Vandecar and Crosson, 1990; Deichmann and Garcia-Fernandez, 1992). The data-processing procedure proposed in this study is robust because: (1) it produces a unique set of electric potentials for arbitrarily complicated survey geometries, (2) it naturally incorporates error statistics and model constraints, (3) it can efficiently process data in real time as they are collected, and (4) it reduces to traditional methods in the absence of survey complexity.

There are numerous examples of SP surveys with interconnected acquisition lines that would apparently benefit from this technique (e.g., Corwin and Hoover, 1979; Michel and Zlotnicki, 1998; Finizola et al., 2003; Yasukawa et al., 2003; Aizawa, 2004), though this topic is not discussed explicitly in these papers. All of these studies involve a relatively large survey area (~0.3 km^2 to more than 20 km^2) with limited roads or paths along which measurements are taken, in addition to sometimes rough terrain in the vicinity of volcanic systems, which necessitates the use of multiple, interconnected survey lines. When two closed acquisition loops share two or more common measurement locations, their crossover errors are no longer independent, and the final survey map will depend on the order in which the lines are processed. This can become significant when there are many intersecting survey lines with multiple crossover points, as will be illustrated in a field-data example in this paper.

Our proposed method produces a unique solution for the electric-potential field by processing all of the collected data simultaneously in a survey-consistent approach. Measurements are expressed as a linear system of equations, and the entire system is solved to minimize the misclosures over the entire survey. Ordinary least squares, which minimizes the l_2 norm of the difference between measured and predicted data, is the simplest approach to this problem. We also explore the use of an l_1 measure of misfit, which can be more robust in the presence of unreliable measurements (Claerbout and Muir, 1973; Farquharson and Oldenburg, 1998) that can occur with SP surveys, but is computationally more expensive.

SP DATA ACQUISITION

Values of the electric potential in an SP survey are given with respect to an arbitrary reference station, which is typically assigned a value of 0 mV for convenience. When possible, it is preferable to measure the potential between each survey station and the fixed reference with a variable length of wire, directly measuring the potential field and eliminating the need for extra processing. When surveys span large areas over rough terrain, however, the length of wire that can be deployed at one time is often limited. In this case, measurements are made with respect to a single reference until the maximum amount of wire is deployed. This last survey location then becomes the new reference, and measurements continue from this point. The electric potential measured at the second reference site from the original reference must be added to each of the potentials measured relative to the second reference station. In this fashion, multiple lines can be tied together to cover large areas using successive references (e.g., Telford et al., 1990).

A limiting case of this method is called the gradient configuration, where a fixed length of wire equal to the minimum station spacing is used. The difference in electric potential is measured between the two stations, and then both electrodes move forward one wire length so that the rear electrode takes the position of the front electrode during the previous measurement. Again, starting from a reference value of 0 mV at the first station, the potential differences are integrated along the survey line to compute the potential at each survey point with respect to the reference.

Two electrodes in direct contact with one another should have no potential difference between them. In practice, however, electrode drift can result in a small potential difference between electrodes (sometimes up to a few millivolts) when they are in direct contact. Unaccounted for, this small difference can produce large cumulative errors using the gradient method, as the bias is integrated over many measurements. Of course, this depends on the magnitude of the anomaly of interest, which can vary from tens to hundreds of millivolts, depending on the application and geologic setting (Telford et al., 1990). Another possible systematic source of error involves telluric currents, which can result in measurable potentials when the electrode separation is relatively large (several millivolts per kilometer). Random errors associated with electrode contact, instrumentation, and cultural noise are also important to consider (e.g. Corwin and Hoover, 1979).

Kirchhoff's voltage law requires that the total potential drop ($\Delta \mathbf{v}$) around any closed survey loop (l) must equal zero,

$$\int \Delta \mathbf{v} \cdot \mathbf{dl} = 0. \tag{1}$$

Because of measurement errors, however, this does not always occur, and a mis-tie is manifested at the closure point. A common means of accounting for this is to evenly distribute the misclosure errors for each loop among the measurements in that loop (Corwin, 1990). This is a useful way to account for accumulated errors, but can become complicated if multiple connected loops share segments.

Note that distributing the loop-closure error evenly among the measurements is strictly only correct when the actual measurement errors are all equal (systematic), such as the case with a constant po-

tential difference between the measuring electrodes caused by drift. If the errors are purely random, this amounts to distributing the mean error along the loop to each measurement. Therefore, it is generally beneficial to form many closed loops that share segments in order to gain additional measures of the errors along each loop. In the limiting case, the survey would consist of a complete grid where every measurement belongs to multiple loops such that the closure errors can be associated with a single measurement, rather than being distributed over multiple measurements (Bandy et al., 1990).

There is a sequence implied in the traditional method of collecting and processing data described above: each line of data is processed individually, lines are tied together at their intersections, and loop-closure errors are distributed as they are incurred. An SP survey with interconnected tie-points and loops that share segments can no longer be processed sequentially because the loops are not independent. Numerous solutions for the potential field can be found simply by processing lines of data in different order. Our proposed method for calculating the potential field accounts for all data points simultaneously, thereby eliminating this problem, and measurement statistics or model constraints can easily be incorporated into the procedure.

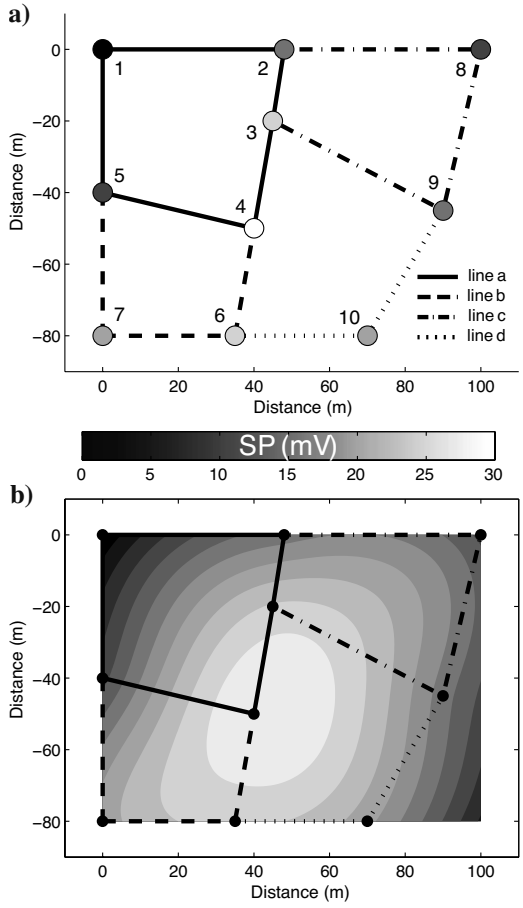

Figure 1. Synthetic example of a gradient SP survey with 10 stations and 13 measurements (based on Cowles, 1938). (a) Symbol shading represents the true station potentials. Gradient data are simulated along four lines (a-d) by calculating potential differences between adjacent stations. (b) Interpolated potential field using the 10 stations in (a).

METHODOLOGY

A simple synthetic example fashioned after that of Cowles (1938) is used to illustrate the methodology for calculating the potential field from a set of gradient SP measurements. Figure 1a shows an example with 10 stations, where the shade of the marker at each station indicates the true potential at each point. An interpolated map of the potential field is illustrated in Figure 1b. Synthetic, noise-free, gradient SP data are calculated by taking the difference between adjacent potentials for each of the 13 measurements along four traverses (a-d), indicated by the different line styles that connect points. Each traverse forms a closed loop, and no measurements are repeated. That is, the potential between stations 4 and 5 is measured on line a, and therefore does not need to be remeasured on line b. The simulated field data are summarized in Table 1.

A critical bookkeeping step requires that each station is assigned a unique number, even though some stations are used for more than one measurement. In practice, station numbers are incremented by one at each new measurement location. When a new measurement ties into a station already used on a previous line, it is important to record the original station number.

Given $M = 13$ measurements and $N = 10$ stations in this example, the relationship between the unknown potentials ($\mathbf{v} = [v_1 \ldots v_N]^T$) and measured gradients ($\mathbf{d} = [\Delta v_1 \ldots \Delta v_M)]^T$) can be written as a system of linear equations,

$$\mathbf{A}\mathbf{v} = \mathbf{d} + \mathbf{e}, \tag{2}$$

where $\mathbf{e}$ is a vector of the unknown measurement errors. $\mathbf{A}$ is the connectivity (or topology) matrix that describes the acquisition geometry and connects measurements to their uniquely numbered stations. The connectivity matrix is sparse and contains only 1, -1, and 0 entries. Each measurement produces one row in $\mathbf{A}$:1 is placed in the column corresponding to the unique station number for the front electrode, -1 in the column corresponding to the rear-electrode station number, and 0 in the remaining columns. When each row is mul-

Table 1. Simulated SP data set for the synthetic example in Figure 1.

Measurement number	Survey line	Rear-electrode station # (j)	Front-electrode station # (i)	Measured SP (mV)
1	a	1	2	15
2	a	2	3	10
3	a	3	4	5
4	a	4	5	−20
5	a	5	1	−10
6	b	4	6	−5
7	b	6	7	−5
8	b	7	5	−10
9	c	2	8	−5
10	c	8	9	5
11	c	9	3	10
12	d	9	10	5
13	d	10	6	5

tiplied by **v**, the result is a simple expression for a potential difference, $v_i - v_j$, associated with the measured value $\mathbf{\Delta}v$ in the same row of **d**.

Because only differences are involved in each measurement, all of the rows of **A** add up to zero; therefore, the columns are not linearly independent, and the potentials can only be determined up to an arbitrary constant. By assigning a value (typically 0 mV) to the global reference point for the survey, column **A** associated with the reference location is removed. This guarantees that the number of data is at least equal to (and possibly greater than) the number of unknown parameters, depending on whether survey lines form closed loops. As long as all of the survey stations are connected through one or more reference locations, the problem of determining the potential field relative to a global reference point is a well-posed problem.

We define an objective function (Φ) that is a measure of data misfit (ϕ_d) plus a regularization functional (ϕ_m) using the l_2 norm:

$$\Phi(\mathbf{v}) = \phi_d + \phi_m = \|\mathbf{W}_d(\mathbf{d} - \mathbf{A}\mathbf{v})\|_2^2 + \lambda\|\mathbf{W}_m\mathbf{v}\|_2^2. \tag{3}$$

$\mathbf{W}_d$ is a diagonal data-space weighting operator that incorporates information about the measurement errors, where entries are typically the inverse of the estimated standard deviation for each measurement (i.e., $\mathbf{W}_d = \boldsymbol{\sigma}^{-1}\mathbf{I}$). $\mathbf{W}_m$ is a model-space regularization operator that provides additional model constraints. In this study, we choose $\mathbf{W}_m = \nabla_l^2$ to promote solutions for the potential field that are spatially smooth, where ∇_l is the gradient in the direction of the acquisition line. $\mathbf{W}_m$ can, therefore, be computed for arbitrary station spacing $\mathbf{\Delta}x_i$ where

$$\mathbf{W}_m = \mathbf{A}^T\mathbf{X}^2\mathbf{A}, \tag{4}$$

and

$$X_{ij} = \begin{cases} (\Delta x_i)^{-1} & i = j \\ 0 & i \neq j \end{cases}. \tag{5}$$

Here, the subscripts i and j are used to form a diagonal operator, with nonzero elements defined by the inverse of the ith station spacing. λ is a trade-off parameter that provides a balance between data misfit and model smoothness. Minimization of equation 3 by setting $\partial\Phi(\mathbf{v})/\partial\mathbf{v} = 0$ results in a linear system of equations that produces an estimate of the potential field, $\hat{\mathbf{v}}$,

$$(\mathbf{A}^{\mathrm{T}}\mathbf{W}_d^2\mathbf{A} + \lambda\mathbf{W}_m^T\mathbf{W}_m)\hat{\mathbf{v}} = \mathbf{A}^{\mathrm{T}}\mathbf{W}_d^2\mathbf{d}. \tag{6}$$

The model regularization term, ϕ_m, is not strictly required to provide a stable inversion result, but is used to prevent overfitting the data in the presence of noise. We compute ϕ_d for multiple values of λ, and interpolate to find the value of the trade-off parameter that results in a data misfit equal to a preselected target-misfit value, ϕ_d^{tar}. Assuming Gaussian measurement errors with known standard deviation, we use a target misfit value equal to the number of measurements, M. Alternatively, one could use the L-curve method (e.g., Hansen, 1992) to choose a value for λ that provides a trade-off between ϕ_d and ϕ_m.

For the synthetic example in Figure 1, we add Gaussian noise with $\sigma = 2.5$ mV (30% of the mean of the absolute value of the noise-free data) to the 13 synthetic measurements. Figure 2 shows the result of implementing equation 6 with $\lambda = 0.022$ so that $\phi_d = \phi_d^{\mathrm{tar}} = 13$. The inversion successfully recovers the original potential field such that it is able to predict the measured data within the expected errors, as can be seen in Figure 2a and b.

Cowles' (1938) approach to closing slope (gradient) data traverses using least squares is equivalent to the methods proposed here. Instead of the connectivity matrix, however, an edge-loop matrix is used to represent the four independent loops in the survey. The four parameters found by inverting this matrix are Lagrange multipliers, and linear combinations of them produce the minimal slope-correction terms that are equal to the elements of $(\mathbf{d} - \mathbf{A}\hat{\mathbf{v}})$. The corrected slopes are found such that the loop-closure errors are minimized, which produces the same potential field as the connectivity-matrix method. The two methods are essentially the same; the only difference is in their application. The connectivity-matrix approach presented in this paper is appropriate for geophysical surveys because it can be constructed efficiently as data are collected, while finding the independent loops in a complicated network may not be obvious.

One drawback to the commonly used l_2 norm is the strong influence of outliers on the solution. There are numerous mechanisms that can result in large measurement errors during an SP survey, such as cultural noise, poor electrode contact, or strong near-surface heterogeneity. An alternative approach to the mis-tie problem, though slightly more computationally expensive, is to use an l_1 measure of

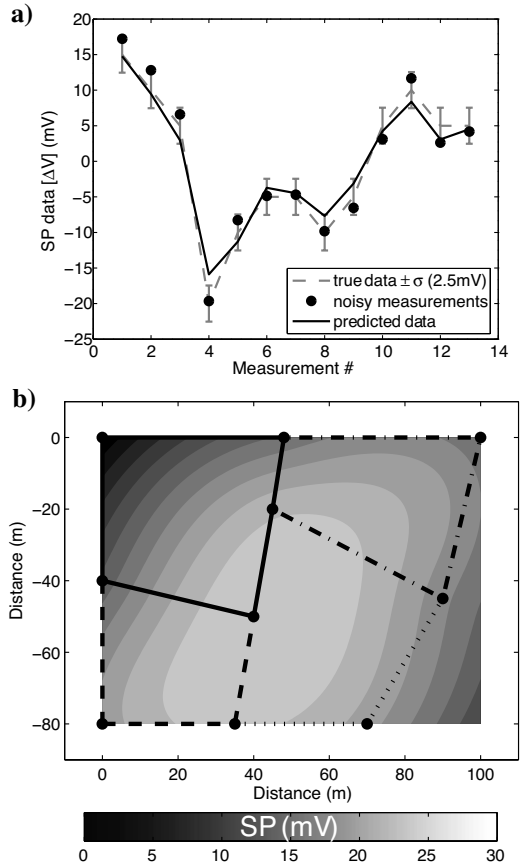

Figure 2. Illustration of the l_2 inversion results for the data from Figure 1 with additional Gaussian noise. The inversion method is able to successfully predict measurements within the expected errors. (a) True data that would be measured from the potentials in Figure 1a (gray line) with error bars to denote the standard deviation of the added noise (2.5 mV), and one realization of synthetic measurements with noise added (black dots). (b) Interpolated potential field found by inverting the noisy measurements.

data misfit, which is less sensitive to erratic measurements (Claerbout and Muir, 1973). This requires an iterative-solution technique (Schlossmacher, 1973; Scales et al., 1988), sometimes referred to as iteratively reweighted least squares (IRLS), whereas the l_2 method can be solved in a single step. We follow the method of Farquharson and Oldenburg (1998) to define a set of linear equations, similar to equation 6, that minimize the objective function using an l_1 norm. The details of this approach are presented in Appendix A, and a synthetic example is presented in the next section that compares the use of the l_1 and l_2 measures of misfit.

APPLICATION TO A SYNTHETIC EXAMPLE USING THE L_1 NORM

A larger synthetic example is used to illustrate the utility of the l_1 measure of data misfit for the SP survey mis-tie problem, particularly when the measurements contain outliers. The MATLAB® peaks function is used as the true potential field for this example, shown in Figure 3a, where the range of approximately 140 mV is typical of many SP surveys. Peaks is a predefined, smoothly varying function of the two coordinates, and has the general appearance of a typical SP map that makes it appropriate for this example. The units of distance are arbitrary because we are only interested in potential differences between survey stations.

A grid of six survey lines (a-f) is used to simulate an SP survey, which are also marked on the figure. Each line consists of 49 stations, though several stations are repeated on multiple lines at the intersection points, giving a total of $N = 285$ unique stations. The station potentials ($\mathbf{v}^{\text{true}}$) sampled from the true potential field in Figure 3a are illustrated in Figure 3b. An SP survey is simulated using the gradient method along each survey line, so that the data represent potential differences between adjacent stations.

Figure 3c shows the synthetic SP data ($\mathbf{d}$) along each line, with a total of $M = 288$ measurements. First, purely Gaussian noise with $\sigma = 0.96$ mV (30% of the mean of the absolute value of the noise-free data) is added to the measurements. $\mathbf{A}$, $\mathbf{W}_d$, and $\mathbf{W}_m$ are constructed according to the methods discussed in the methodology section of this paper. In the first iteration, equation 6 is solved with $\lambda = 1.48$ to provide the target l_2 misfit, $\phi_d^{\text{tar}}(l_2) = 288$, yielding $\hat{\mathbf{v}}^1$. This solution is used to compute the l_1 estimate according to the iterative methods outlined in Appendix A, with $\phi_d^{\text{tar}}(l_1) = 229.8$. This value comes from Parker and McNutt (1980), who define an appropriate value for the target data misfit using the l_1 measure as $\phi_d^{\text{tar}}(l_1) = \sqrt{2/\pi}M$ when only Gaussian noise with known data variance is present. A stopping criterion is set such that the inversion ends when the average difference between successive model estimates is less than 0.5%.

One procedural difference is that the model reweighting matrix is held constant ($\mathbf{R}_m = \mathbf{I}$) throughout the iterative process. Maintaining the l_2 measure for the model regularization term produces a smoother solution than when the reweighting scheme is used. This is appropriate since our goal is to recover a smooth solution, though it amounts to the incorporation of somewhat arbitrary prior information into the inversion. The objective function that is minimized is, therefore,

$$\Phi(\mathbf{v}) = \phi_d + \phi_m = \|\mathbf{W}_d(\mathbf{d} - \mathbf{A}\mathbf{v})\|_1^1 + \lambda\|\mathbf{W}_m\mathbf{v}\|_2^2. \tag{7}$$

Figure 4 shows the inversion results for this example, where data from all six lines are plotted in succession according to the station or measurement number. Figure 4a compares the noise-free (light-gray line) and noisy (gray dots) data with the predicted data ($\mathbf{A}\hat{\mathbf{v}}$) for the l_2 (dotted-black line) and l_1 (dashed-black line) inversion results. In this example with no outliers, there is little difference between the two solutions, and the predicted data curves both follow the true data curve fairly well. Figure 4b shows the true station potentials along

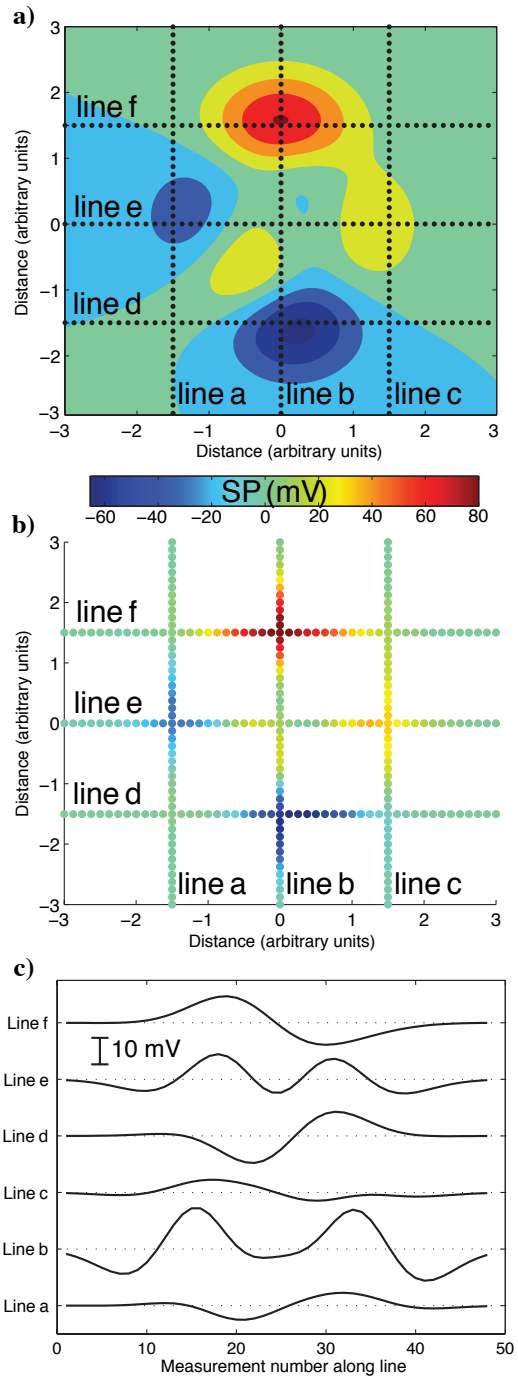

Figure 3. Synthetic potential field used to illustrate mis-tie methods. (a) Map of the complete potential field with six survey lines annotated. (b) True potentials at the survey stations (49 stations per line, 294 stations in total). (c) Synthetic-gradient data (potential differences between adjacent stations) for each of the survey lines.

with the potentials predicted by the l_2 and l_1 inversions. In general, both results do a good job of reproducing the true potential field, though the l_2 results are slightly better when compared with the noise-free solution. The model rms error,

$$\text{RMSE} = \sqrt{\frac{\sum_{i=1}^{N} (v_i - v_i^{\text{true}})^2}{N}}, \quad (8)$$

is 2.6 mV for the l_2 result and 5.1 mV for the l_1 result.

Next, we illustrate the effect of outliers in the data by increasing the level of noise at 10% of the measurement locations, chosen randomly throughout the survey. At these locations, $\sigma = 4.8$ mV, which is five times the standard deviation of the noise for the rest of the measurements. No prior knowledge about the outliers is assumed, so the same values for the data-weighting matrix and target misfit are maintained as in the previous example ($\mathbf{W}_m = 0.96^{-1}\mathbf{I}$, $\phi_d^{\text{tar}}(l_2) = 288$, and $\phi_d^{\text{tar}}(l_1) = 229.8$). In general, one might need to increase the value of the target misfit when outliers are present in order to avoid overfitting the data. The inversion runs for 21 iterations before the model changes are small enough to meet the stopping criterion, which is similar to the case without outliers that runs for 25 iterations.

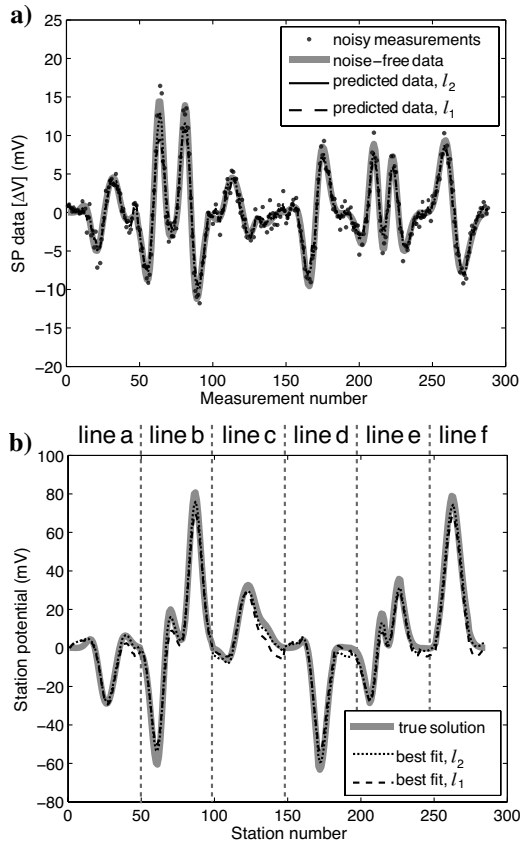

Figure 4. Inversion results for the case with Gaussian noise only ($\sigma = 0.96$ mV). All six lines are displayed sequentially as a function of survey measurement or station number. (a) Comparison of the synthetic noise-free (light-gray line) and noisy (gray dots) data with data predicted by the l_2 inversion (black-dotted line), and the l_1 inversion (black dashed line). (b) Comparison of the true station potentials (light-gray line) with the results from the l_2 inversion (black-dotted line), and the l_1 inversion (black-dashed line).

Figure 5 shows the inversion results for the case with unexpected erratic data. In Figure 5a, the difference between the l_2 (dotted-black line) and l_1 (dashed-black line) penalties on the data residual is apparent. As expected, the l_2 result tends to overfit the data caused by the quadratic penalty on the residuals. Several locations where this is most evident are highlighted by black arrows. Figure 5b shows the corresponding station potentials predicted by the two inversion methods compared with the true solution. Large errors in the potentials of up to ~20 mV can be seen in the l_2 solution, while the l_1 solution avoids these artifacts. Quantitatively, the model errors according to equation 8 are 7.8 mV and 4.7 mV for the l_2 and l_1 solutions, respectively. Compared with the previous example where there were no outliers, the l_2 model error has tripled, while the l_1 model error has decreased slightly. This comparison somewhat under-represents the success of the l_1 result that is observed in Figure 5b, however, since equation 8 provides the mean model error over all stations, and the greatest improvements occur at a limited number of stations.

These results confirm the general behavior that we expect: the l_1 measure of misfit produces a more robust solution in the presence of outliers. In the case where the data contain only Gaussian noise, the

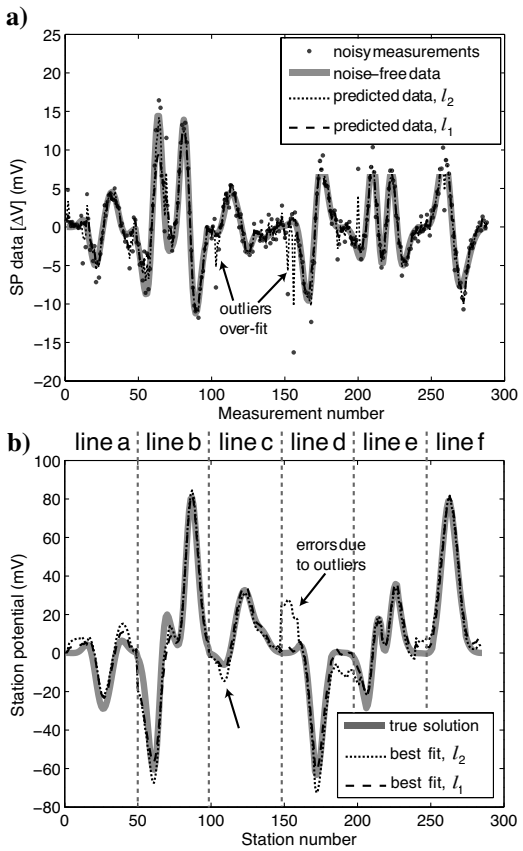

Figure 5. Inversion results for the case where 10% of the measurement locations have an unexpectedly large measurement error ($\sigma = 4.8$ mV) to simulate outliers. All six lines are displayed sequentially as a function of survey measurement or station number. (a) Comparison of the synthetic noise-free (light-gray line) and noisy (gray dots) data with data predicted by the l_2 inversion (black-dotted line), and the l_1 inversion (black-dashed line). (b) Comparison of the true station potentials (light-gray line) with the results from the l_2 inversion (black-dotted line), and the l_1 inversion (black-dashed line). Black arrows highlight several of the locations most affected by the outliers.

l_1 and l_2 measures of misfit produce similar solutions. There are a few locations where the l_2 solution provides a slightly better result in both examples, though the improvements are not dramatic considering the level of noise. The extra computational cost for the l_1 method arises from solving equation A-5 multiple (often ~10 to 20) times, but is by no means prohibitive.

SP FIELD EXAMPLE FROM NEVIS, WEST INDIES

Background

An SP survey was carried out on the island of Nevis (Figure 6) in August 2004 as a part of a larger geothermal-exploration campaign supported by the Organization of American States (OAS) Geo-Caraïbes program aimed at developing geothermal energy in the Eastern Caribbean. Nevis is a small (93 km^2) island that is part of the Federation of St. Kitts and Nevis, located at 17°9N, 62°35W, approximately 350 km southeast of Puerto Rico. Nevis' immediate neighbors are St. Kitts to the north and Montserrat to the south. The island's topography is dominated by Nevis Peak, a stratovolcano in the center of the island with an elevation of 985 m. There is no historic record of volcanic activity on Nevis; in their report on geothermal resources in the Eastern Caribbean, Geotermica Italiana (1992) provides a K-Ar date of 0.1 ± 0.06 Ma for a small dome at the top of Nevis Peak, which may be the youngest volcanic feature on the island.

There are several pieces of modern-day evidence for a viable geothermal resource on Nevis. The underlying heat source is hypothesized to be a magma body located beneath the island, which is supported by multiple seismic swarm events (Willmore, 1952; Robson et al., 1962) and geochemical information (Pedroni et al., 1999). Additionally, there are a number of boreholes and springs with elevated water temperatures (up to 46° C), mostly located on the west side of the island north of Charlestown (Kennedy and Robins, 1988). Geotermica Italiana (1992) summarizes several areas of fumerolic activity, also on the west side of the island, that were documented by previous researchers (Willmore, 1967; Hutton and Nockolds, 1978). One of these is the Farm Estate Soufriere, which is located within our survey area (Figure 6). Temperatures of approximately 100° C have been reported at the soufriere, though the degree of activity has varied over several decades.

The principal goal of the SP survey is to delineate possible regions of active fluid circulation that may not be expressed at the earth's surface. In this paper, we are primarily interested in illustrating the efficacy of our proposed data-processing methods, using this field-survey example to produce a reliable SP map. Future research will involve a more comprehensive analysis of the SP data using the inversion techniques discussed by Minsley et al. (2007a). This will be combined with other geophysical, geologic, and geochemical information to form a more complete representation of the geothermal system.

Data collection and analysis

The data were collected using the gradient-electrode configuration with a fixed separation of about 75 m. An area of approximately 16 km^2 was covered by 19 lines of data collected along accessible roads and trails in the southwest part of the island. The data set consists of 483 potential-difference measurements using 469 unique stations. The lines of data make up a complicated network of measurements with many interconnected loops (Figure 6). The data were corrected for electrode drift by periodically placing the two electrodes in direct contact, and subtracting this drift potential from the measured data. Telluric corrections were deemed unnecessary, though they may remain a small source of error in the data. Difficulties in calculating a unique potential field by sequentially tying lines together and distributing closure errors necessitated the survey-consistent approach developed in this paper.

Figure 7 highlights the benefit of using the survey-consistent method discussed in the methodology section of this paper to minimize the loop-closure errors globally, rather than the traditional method of processing lines sequentially. This figure shows three different calculations of the station potentials interpolated over the whole survey area, where individual lines of data were processed in

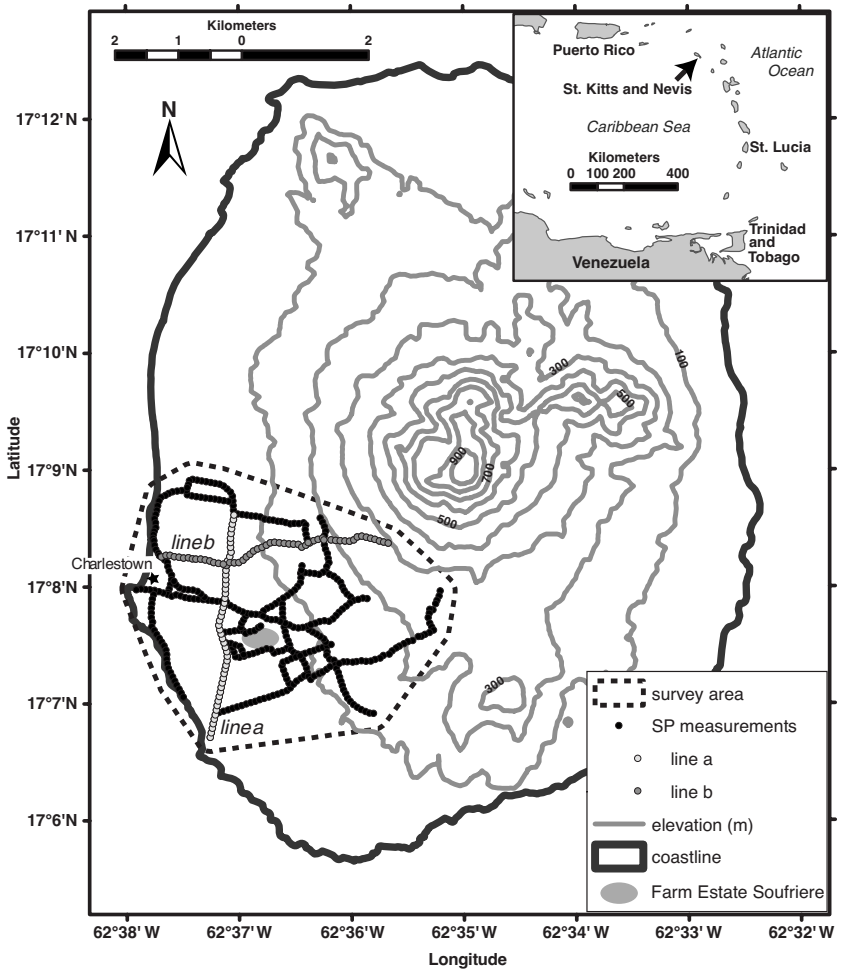

Figure 6. Map of Nevis showing the station locations for 19 lines of gradient SP data over an area of approximately 16 km^2 in the southwest part of the island. The two lines with different shading (lines a and b) are used for displaying results in subsequent figures.

different sequences. This technique results in nonindependent loop closures and significantly different images, depending on the arbitrary order in which the data are processed.

Next, the drift-corrected SP data are inverted using the methods developed in this paper. In this field study, as with many geophysical surveys, we do not know the true standard deviation of the measurement errors, or to what extent outliers are present in the data. We therefore show several inversion results using different combinations of values for $\mathbf{W}_d = \sigma^{-1}\mathbf{I}$ and ϕ_d^{tar} to get a sense of the range of possible solutions. Each inversion assumes a constant value of σ (either 2 or 5 mV) for all measurements, and two possible values for the target data misfit. The target misfit is set to $\phi_d^{\text{tar}}(l_2) = M = 483$ and $\phi_d^{\text{tar}}(l_2) = 1.5M = 724.5$ for the l_2 inversions, and $\phi_d^{\text{tar}}(l_1) = \sqrt{2/\pi}M = 385.4$ and $\phi_d^{\text{tar}}(l_1) = 1.5\sqrt{2/\pi}M = 578.1$ for the l_1 inversions. Thus, four different solutions are computed for each of the l_2 and l_1 methods.

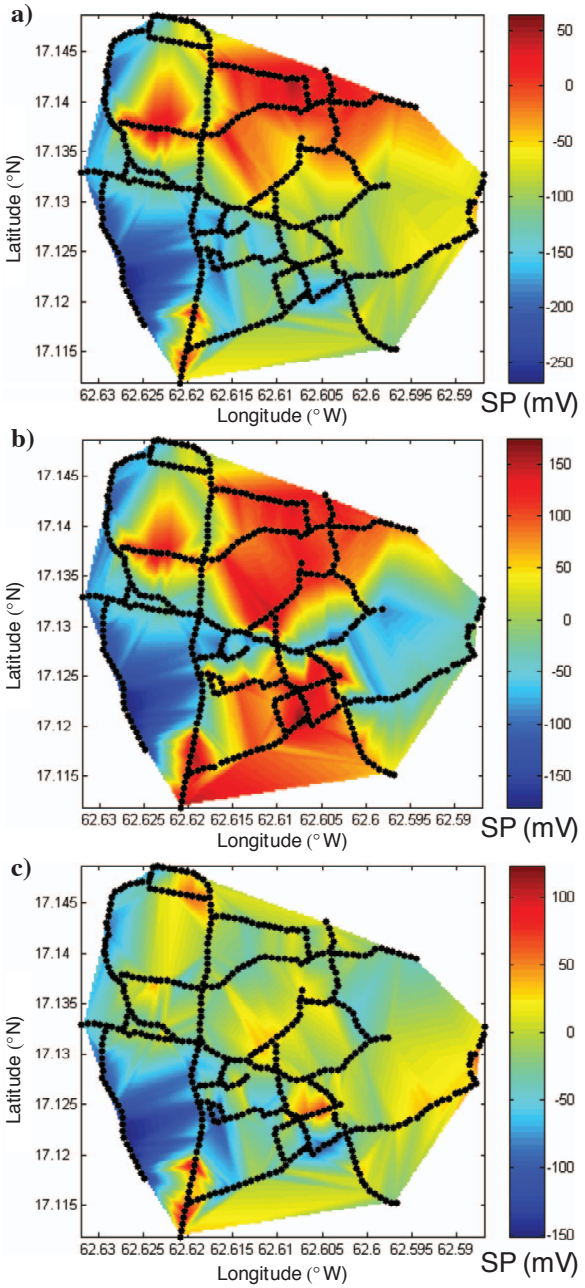

Figure 7. Three different versions of the potential field computed using traditional processing methods with lines of data processed in different orders, then interpolated over the entire survey area. Loop-closure errors are distributed along new loops as they are completed, but potentials along existing loops are not modified. Because the loops are not independent, this methodology produces inconsistent results.

Figure 8 illustrates the inversion results extracted along two of the longest survey lines, labeled lines a and b in Figure 6. In Figure 8a, the measured SP data (black dots) are compared with the predicted data ($\mathbf{A}\hat{\mathbf{v}}$) for the l_2 (black-shaded line) and l_1 (gray-shaded line) inversions. The width of each line represents the range of results from the four different cases of target data misfit and assumed-measurement standard deviations, while the white-dashed line represents the mean result. Inverted station potentials ($\hat{\mathbf{v}}$) along these two lines are shown in Figure 8b. The width of each shaded area again represents the range of solutions recovered from the four different inversion runs, and the white-dashed line is the mean result. The range of possible solutions is generally larger for the l_1 results because of the weaker constraint on the data misfit for this method.

The l_2 and l_1 solutions mostly follow the same trends, though there is a spatially variable offset between the two results because of the

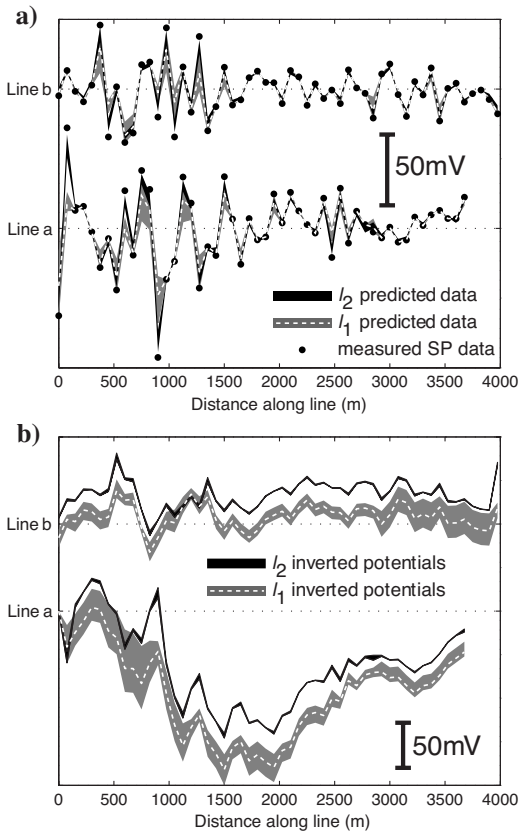

Figure 8. Inversion results for the field data set shown along lines a and b from Figure 6. The width of each filled area represents the range of results that are found using different combinations of σ and ϕ_d^{tar} for the l_2 and l_1 measures of misfit, while the white-dashed line represents the mean result. (a) Comparison of the field SP measurements (black dots) with predicted data ($\mathbf{A}\hat{\mathbf{v}}$) from the l_2 (black area) and l_1 (gray area) inversions. (b) Range of station potentials predicted along the two transects for the different combinations of σ and ϕ_d^{tar} for the l_2 and l_1 measures of misfit.

effect of outliers on the inversion. This can be explained by considering a single line of potential-difference data that is integrated to compute the station potentials, with a single data outlier in the middle of the line. The l_2 potentials will have a large step jump at the location of the outlier, whereas the l_1 potentials, which avoid integrating the outlier, will not have the step jump. Therefore, the two results will be similar up to the location of the outlier, but will be offset by a constant value (equal to the magnitude of the outlier) for the remainder of the line. The results in Figure 8 are somewhat more complicated because the entire survey is inverted simultaneously, and the shifts in Figure 8b can be caused by outliers in Figure 8a as well as outliers from other survey lines.

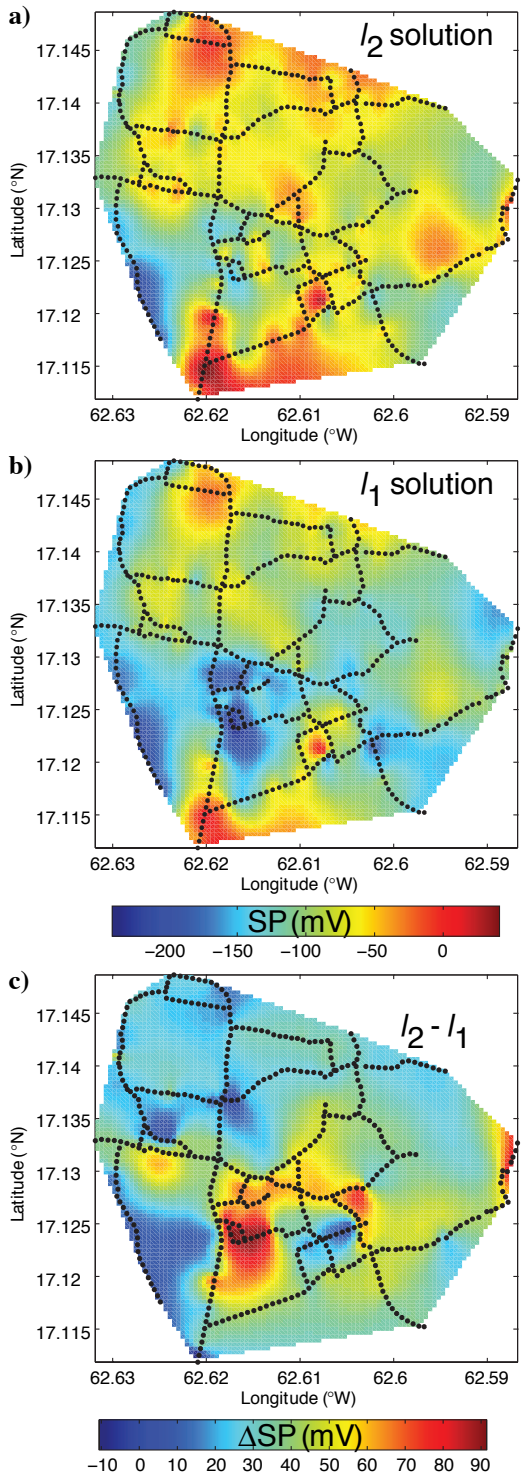

Figure 9. Potential-field maps calculated using the l_2 (a) and l_1 (b) inversion methods, interpolated over the entire survey area. In both cases, the mean result from using four different combinations of data weights and target-misfit values is illustrated, which corresponds to the white-dashed lines in Figure 8. (c) The difference between the mean l_2 and l_1 solutions varies in magnitude over the entire survey area, but is almost always positive.

Figure 9a shows the mean l_2 inverted potential field interpolated over the entire survey area, and Figure 9b shows the mean l_1 result using the same color scale. As noted in Figure 8b, the two solutions have a similar trend, but are offset at most survey locations, with an average value of approximately 35 mV over the entire survey area. There are specific regions where the two solutions are significantly different, such as the increased (~50 mV) broad negative anomaly for the l_1 result along line a from around 1000–2500 m relative to the start of the line (0 m), where the potentials for the l_1 and l_2 results are the same (Figure 8b). This increased negative anomaly is clearly evident in Figure 9b and c over several survey lines in the area between 62.61°W-62.62°W and 17.12°N-17.13°N. This is in the general vicinity of the Farm Estate Soufriere, and may be indicative of increased fluid circulation at depth in this area. There are no clear surface manifestations of any of the other SP anomalies, which may also be associated with subsurface-fluid circulation, but further geophysical investigation or drilling is needed to confirm this.

Note that the linear interpolation used to generate the original results in Figure 7 produces less-smooth images than the interpolation used to generate Figure 9. While this accounts for some of the visual differences between figures, the main effect is caused by the difference in inversion methods. We conclude that the survey-consistent approach, whether using the l_2 or l_1 measure of misfit, provides a significantly more robust approach to processing SP data because it results in a unique map that corresponds to the minimum survey-wide closure error.

CONCLUSIONS AND FUTURE WORK

SP surveys acquired with interconnected survey loops require processing techniques that account for the fact that loop-closure errors are not independent. The methodology presented in this paper provides a simple and robust procedure for computing potentials in a survey-consistent fashion. This method is valid for arbitrarily complicated survey geometries, and is equivalent to traditional line-by-line processing methods when survey loops are not interconnected. Our development has involved only SP surveys, though this approach can easily be adapted to other geophysical potential-field methods, such as gravity and magnetics.

Formulated as a linear inverse problem, this technique can easily incorporate statistical information regarding measurement errors and model constraints based on prior information. Additionally, we have shown the utility of solving the problem using an l_1 measure of misfit when outliers are present in the data. The l_1 and l_2 solutions produce similar results when the noise is solely Gaussian, though the former case requires an additional computational cost to solve the problem iteratively.

These methods can be readily adapted to provide a real-time SP mapping system. A handheld personal computer with a global-positioning system (GPS) antenna and data logger can record potential differences at stations in the field. The topology matrix ($\mathbf{A}$) can, therefore, be constructed as the data are collected, and updated SP maps can be computed at any time. Even for relatively large surveys with several hundred stations, the computation time will be on the order of several minutes. This information can be used immediately to make decisions regarding where more data should be collected.

ACKNOWLEDGMENTS

We thank Mark Lambrides and the Organization of American States for supporting the field component of this study carried out in Nevis. Additionally, we are grateful to the other members of the geophysical-survey team: Mary Krasovec, Colin Morgan, and Timur Kanachet. GPS survey positions were provided by Richard Robertson and Rosemarie Mohais of the Seismic Research Unit, University of West Indies, Trinidad. We appreciate the input of Colin Farquharson, two anonymous reviewers, and the associate editor during the review of this paper.

APPENDIX A

MINIMIZING SURVEY MIS-TIES USING AN l_1 MEASURE OF DATA MISFIT

We define an objective function (ϕ) to be minimized using an l_1 measure that is the sum of absolute values of a vector, $\mathbf{x}$,

$$\phi(\mathbf{x}) = \sum_j |x_j|. \tag{A-1}$$

This provides a framework for minimizing a general objective term using the l_1 measure, where $\mathbf{x}$ can represent either the data-misfit term,

$$\mathbf{x} = \mathbf{W}_d(\mathbf{d} - \mathbf{A}\mathbf{v}), \tag{A-2}$$

or a measure of model length given by a regularization functional,

$$\mathbf{x} = \mathbf{W}_m\mathbf{v}. \tag{A-3}$$

A modified form of the objective function

$$\phi(\mathbf{x}) = \|(\mathbf{x}^2 + \varepsilon^2)^{1/2}\|_1^1 \tag{A-4}$$

is utilized in order to avoid the discontinuity in $\partial\phi/\partial\mathbf{x}$ for any $x_i = 0$ (Ekblom, 1987; Farquharson and Oldenburg, 1998). A small user-specified value, ε, introduces stability for the case where any $x_i = 0$.

The chain rule is used to compute the derivative of the objective function with respect to the unknown potentials, $\mathbf{v}$. Setting this expression equal to zero results in a new system of equations that provides an estimate of the unknown potentials,

$$(\mathbf{A}^T\mathbf{W}_d\mathbf{R}_d\mathbf{W}_d\mathbf{A} + \lambda\mathbf{W}_m\mathbf{R}_m\mathbf{W}_m)\hat{\mathbf{v}} = \mathbf{A}^T\mathbf{W}_d\mathbf{R}_d\mathbf{W}_d\mathbf{d}, \tag{A-5}$$

where

$$R_{ij} = \begin{cases} (x_i^2 + \varepsilon^2)^{-1/2} & i = j \\ 0 & i \neq j \end{cases}. \tag{A-6}$$

Because $\mathbf{R}$ is a function of the unknown potentials, this is a nonlinear system, and an iterative approach must be used. This is sometimes referred to as IRLS (Scales et al., 1988).

We again follow the approach of Farquharson and Oldenburg (1998) by setting $\mathbf{R} = \mathbf{I}$ for the first iteration, which results in the traditional least-squares solution given by equation 6. This estimate, $\hat{\mathbf{v}}^k$ ($k = 1$), is then used to compute a new $\mathbf{R}^{k+1}$ from equation A-6, which is subsequently substituted into equation A-5 to produce a new estimate, $\hat{\mathbf{v}}^{k+1}$. This procedure is repeated until $|\hat{\mathbf{v}}^{k+1} - \hat{\mathbf{v}}^k| < \delta$, where δ is a user-specified value that determines when to stop the inversion based on the change in model parameters between successive IRLS iterations. Assuming only Gaussian errors and known data variance, an appropriate value for the target data misfit using the l_1 measure is $\phi_d^{\text{tar}}(l_1) = \sqrt{2/\pi}M$ (Parker and McNutt, 1980). In the case where outliers are present, however, a larger target misfit may be needed to avoid overfitting the data.

There are now three user-defined parameters, which are not necessarily independent from one another, that control the behavior of the solution: λ, one ε for $\mathbf{R}_d$, and one ε for $\mathbf{R}_m$. Small values of ε are needed to approximate equation A-1, but too small a value can introduce instability for any $x_i \rightarrow 0$. Large values of ε tend to act more like the traditional regularization parameter, λ (i.e., $\mathbf{R} \rightarrow \varepsilon^{-1}\mathbf{I}$ when $\varepsilon \gg x_i$). Typically, a plot of $\phi(\mathbf{x})$ for a range of ε is used to determine an optimal balance between these extremes (Farquharson and Oldenburg, 1998; Zhdanov and Tolstaya, 2004). This is not computationally expensive because it only requires substituting multiple values of ε into equation A-4 using the current value of $\mathbf{x}$. λ can be chosen in the same fashion that is discussed in the methodology section of this paper, by searching over multiple possible values to find the one that provides the desired data misfit, ϕ_d^{tar}.

An algorithm for solving the SP survey mis-tie problem using the l_1 norm is summarized below:

1. Compute $\mathbf{A}$, $\mathbf{W}_d$, and $\mathbf{W}_m$ as suggested in the methodology section of this paper.
2. Set $\mathbf{R}_d = \mathbf{R}_m = \mathbf{I}$.
3. Solve equation A-5 for multiple values of λ, and find the value that produces $\phi_d = \phi_d^{\text{tar}}$ for the l_2 measure of misfit. The corresponding $\hat{\mathbf{v}}^1$ is the l_2 solution.
4. Choose optimal values of ε for $\mathbf{R}_d$ and $\mathbf{R}_m$ by plotting ϕ_d and ϕ_m using equation A-4 with the current $\hat{\mathbf{v}}^k$ and a range of ε.
5. Compute $\mathbf{R}_d$ and $\mathbf{R}_m$ using equation A-6 with the current $\hat{\mathbf{v}}^k$ and ε.
6. Update $\phi_d^{\text{tar}} = \max[0.95\phi_d^{\text{tar}}, \phi_d^{\text{tar}}(l_1)]$ to provide a smooth transition between the l_2 and l_1 target misfit values.
7. Solve equation A-5 for multiple values of λ, and find the value that produces $\phi_d = \phi_d^{\text{tar}}$. Store the solution $\hat{\mathbf{v}}^k$ that corresponds to the target misfit.
8. Repeat from step 4 until $|\hat{\mathbf{v}}^{k+1} - \hat{\mathbf{v}}^k| < \delta$.

REFERENCES

Aizawa, K., 2004, A large self-potential anomaly and its changes on the quiet Mt. Fuji, Japan: Geophysical Research Letters, **31**, L05612.
Bandy, W. L., A. F. Gangi, and F. D. Morgan, 1990, Direct method for deter-

mining constant corrections to geophysical survey lines for reducing mis-ties: Geophysics, **55**, 885–896.
Bogoslovsky, V. A., and A. A. Ogilvy, 1973, Deformations of natural electric fields near drainage structures: Geophysical Prospecting, **21**, 716–723.
Claerbout, J. F., and F. Muir, 1973, Robust modeling with erratic data: Geophysics, **38**, 826–844.
Corwin, R. F., and D. B. Hoover, 1979, The self-potential method in geothermal exploration: Geophysics, **44**, 226–245.
Corwin, R. F., 1990, The self-potential method for environmental and engineering applications, *in* S. H. Ward, ed., Geotechnical and environmental geophysics, vol. I: SEG, 127–145.
Cowles, L. G., 1938, The adjustment of misclosures: Geophysics, **3**, 332–339.
Deichmann, N., and M. Garcia-Fernandez, 1992, Rupture geometry from high-precision relative hypocenter locations of microearthquake clusters: Geophysical Journal International, **110**, 501–517.
Ekblom, H., 1987, The L_1-estimate as limiting case of an L_p- or Huber-estimate, *in* Y. Dodge, ed., Statistical data analysis based on the L_1-norm 2nd related methods: North Holland, Amsterdam, 109–116.
Farquharson, C. G., and D. W. Oldenburg, 1998, Non-linear inversion using general measures of data misfit and model structure: Geophysical Journal International, **134**, 213–227.
Finizola, A., F. Sortino, J. F. Lenat, M. Aubert, M. Ripepe, and M. Valenza, 2003, The summit hydrothermal system of Stromboli. New insights from self-potential, temperature, CO_2 and fumarolic fluid measurements, with structural and monitoring implications: Bulletin of Volcanology, **65**, 486–504.
Fitterman, D. V., and R. F. Corwin, 1982, Inversion of self-potential data from the Cerro Prieto geothermal field, Mexico: Geophysics, **47**, 938–945.
Foster, M. R., W. R. Jines, and K. van der Weg, 1970, Statistical estimation of systematic errors at intersections of lines of aeromagnetic survey data: Journal of Geophysical Research, **75**, 1507–1511.
Geotermica Italiana, 1992, Exploration for geothermal resources in the Eastern Caribbean: Final Report, Contract TCD CON 15/90-RLA/87/037.
Hansen, P. C., 1992, Analysis of discrete ill-posed problems by means of the L-curve: SIAM Review, **34**, 561–580.
Hutton, C., and S. Nockolds, 1978, The petrology of Nevis, Leeward Islands, West Indies: Institute of Geological Sciences, Overseas Geology and Mineral Resources, 52.
Johnson, R. H., 1971, Reduction of discrepancies at crossing points in geophysical surveys: Journal of Geophysical Research, **76**, 4892–4897.
Kennedy T. B., and N. S. Robins, 1988, Contributions to the UNESCO hydrogeological atlas of the Caribbean Islands, vol. 4: St. Christopher and Nevis: British Geological Survey Technical Report, Hydrology Series, WD/88/30.
Michel, S., and J. Zlotnicki, 1998, Self-potential and magnetic surveying of La Fournaise volcano (Reunion Island): Correlations with faulting, fluid circulation, and eruption: Journal of Geophysical Research-Solid Earth, **103**, 17845–17857.
Minsley, B. J., J. Sogade, and F. D. Morgan, 2007a, Three-dimensional source inversion of self-potential data: Journal of Geophysical Research, **112**, B02202.
———, 2007b, Three-dimensional self-potential inversion for subsurface DNAPL contaminant detection at the Savannah River Site, South Carolina: Water Resources Research, **43**, W04429.
Naudet, V., A. Revil, E. Rizzo, J.-Y. Bottero, and P. Begassat, 2004, Groundwater redox conditions and conductivity in a contaminant plume from geoelectrical investigations: Hydrology and Earth System Sciences, **8**, 8–22.
Parker, R. L., and M. K. McNutt, 1980, Statistics for the one-norm misfit measure: Journal of Geophysical Research, **85**, 4429–4430.
Pedroni, A., K. Hammerschmidt, and H. Friedrichsen, 1999, He, Ne, Ar, and C isotope systematics of geothermal emanations in the Lesser Antilles Islands Arc: Geochimica et Cosmochimica Acta, **63**, 515–532.
Prince, R. A., and D. W. Forsyth, 1984, A simple objective method for minimizing crossover errors in marine gravity data: Geophysics, **49**, 1070–1083.
Revil, A., D. Hermitte, M. Voltz, R. Moussa, J. G. Lacas, G. Bourrie, and F. Trolard, 2002, Self-potential signals associated with variations of the hydraulic head during an infiltration experiment: Geophysical Research Letters, **29**, 1106.
Robson, G. R., K. G. Barr, and G. W. Smith, 1962, Earthquake series in St. Kitts — Nevis 1961–62: Nature, **195**, 972–974.
Sato, M., and H. M. Mooney, 1960, The electrochemical mechanism of sulfide self-potentials: Geophysics, **25**, 226–249.
Scales, J. A., A. Gersztenkorn, and S. Treitel, 1988, Fast L_p solution of large, sparse, linear-systems — Application to seismic travel time tomography: Journal of Computational Physics, **75**, 314–333.
Schlossmacher, E. J., 1973, Iterative technique for absolute deviations curve fitting: Journal of the American Statistical Association, **68**, 857–859.
Sivenas, P., and F. W. Beales, 1982, Natural geobatteries associated with sulfide ore-deposits, 1. Theoretical studies: Journal of Geochemical Exploration, **17**, 123–143.
Suski, B., E. Rizzo, and A. Revil, 2004, A sandbox experiment of self-potential signals associated with a pumping test: Vadose Zone Journal **3**, 1193–1199.
Telford, W. M., L. P. Geldart, and R. E. Sheriff, 1990, Applied geophysics: Cambridge University Press.
Vandecar, J. C., and R. S. Crosson, 1990, Determination of teleseismic relative phase arrival times using multi-channel cross-correlation and least-squares: Bulletin of the Seismological Society of America, **80**, 150–169.
Willmore, P. L., 1952, The earthquake series in St. Kitts—Nevis 1950–51: Nature, **169**, 770–772.
———, 1967, Windward and Leeward B.W. I.: Preliminary notes on soufriere activity in 1951: University of the West Indies Seismic Research Unit, Special Publication Number 11.
Yasukawa, K., T. Mogi, D. Widarto, and S. Ehara, 2003, Numerical modeling of a hydrothermal system around Waita volcano, Kyushu, Japan, based on resistivity and self-potential survey results: Geothermics, **32**, 21–46.
Zhdanov, M., and E. Tolstaya, 2004, Minimum support nonlinear parametrization in the solution of a 3D magnetotelluric inverse problem: Inverse Problems, **20**, 937–952.